DALTON

FULL PAPER

Oxide solubility and Raman spectra of NdF_3–LiF–KF–MgF_2–Nd_2O_3 melts

Evanthia Stefanidaki,[a] George M. Photiadis,[a] Christos G. Kontoyannis,[a,b] Aasmund F. Vik[c] and Terje Østvold[c]

[a] *Institute of Chemical Engineering and High Temperature Chemical Processes – FORTH, P.O. Box 1414, GR-26500, Patras, Greece. E-mail: cgk@iceht.forth.gr*

[b] *Department of Pharmacy, University of Patras, Patras, Greece*

[c] *Department of Chemistry, Norwegian University of Science and Technology, N-7194 Trondheim, Norway*

Received 19th December 2001, Accepted 21st March 2002
First published as an Advance Article on the web 1st May 2002

The solubility of Nd_2O_3 in NdF_3–LiF–MgF_2 melts is about 0.08–0.38 mol% when the NdF_3 concentration varies from 15 to 30 mol% at 900 °C. The solubility increases from 0.13 mol% at 750 °C to 0.22 mol% at 900 °C in the NdF_3–LiF eutectic. When MgF_2 is added to NdF_3–LiF binary melts saturated with Nd_2O_3, the Nd_2O_3 solubility seems to decrease slightly at 30 mol% NdF_3, while a slight increase was observed with 15 mol% NdF_3 in the binary. When dissolving Nd_2O_3 in the NdF_3–LiF eutectic Raman spectroscopy showed that the complex ions $NdOF_x^{(x-1)-}$ and $Nd_2OF_{x+3}^{(x-1)-}$ may form in the melt. The most reasonable candidates seem to be: $NdOF_4^{3-}$ and $NdOF_5^{4-}$ among the mononuclear compounds and $Nd_2OF_{10}^{6-}$, $Nd_2OF_8^{4-}$ among the binuclear complexes.

Introduction

A knowledge of the structural properties of neodymium fluoride–alkali fluoride–magnesium fluoride liquid mixtures and the solubility of N_2O_3 in these mixtures is important to understand the molten salt electrolytic process for the production of Nd metal and Nd–Mg alloys from a fluoride melt. In this work the effect of the dissolution of Nd_2O_3 on the structural properties of liquid NdF_3–AF eutectics (A = Li, K) is examined by Raman spectroscopy, and the solubility of Nd_2O_3 is determined in some of the binary NdF_3–AF and ternary NdF_3–AF–MgF_2 mixtures. In addition, the Raman bands of NdOF(s) are given. The present work follows an earlier similar study on the $NdCl_3$–NdOCl and $NdCl_3$–KCl–NdOCl liquid systems,[1] and the study of M_2O_5 (Nb and Ta) in liquid MF_5–FLiNaK (eutectic LiF–NaF–KF) mixtures.[2,3] A thorough examination of the structure of Al_2O_3, dissolved in AlF_3–AF (A = Li, Na, K) melts studied by Raman, vapour pressure and solubility measurements has also been reported.[4] Few data are available in the literature on the solubility of Nd_2O_3 in NdF_3–LiF melts. J.E. Murphy *et al.*[5] have studied the solubility of Nd_2O_3 in a NdF_3–LiF–CaF_2 electrolyte at 1030 °C. The concentration of NdF_3 was varied from 5 to 20 mol% and the measured solubilities of Nd_2O_3 varied from 3 to 3.9 wt% which, according to the present work, is very high. Solubilities of approximately 2 wt% of Nd_2O_3 in NdF_3(74, 80 and 90 wt% NdF_3)–LiF molten mixtures and in NdF_3–LiF (50 mol%) at 1000 °C are also reported.[6,7]

Experimental

Chemicals and materials

The LiF (99.5% Alfa, Germany) and KF (Zur analyse, Merck, Germany) were re-crystallised twice under an argon atmosphere from their melts by slow cooling (3 °C h^{-1}) in a glassy carbon crucible, and the oxygen content in the final LiF, detected by LECO TC-436, was 0.0141 wt%. In the purified KF it was much lower. The Nd_2O_3 (99.99%, Alfa, Germany), NdF_3 (99.99%, Merck, Germany) and MgF_2 (99.9%, Alfa, Germany) were dried under vacuum by slowly increasing the temperature up to 500 °C. Within the temperature range 70–200 °C, the NdF_3 and MgF_2 were heated very slowly (3 °C h^{-1}) so that the moisture could be removed before any oxyfluorides formed. The oxygen contents in the final NdF_3 and MgF_2, as measured by LECO TC-436, were found to be 0.089 and 0.0039 wt%, respectively. Powder NdOF was synthesized by heating an equimolar mixture of NdF_3 and Nd_2O_3 at 1100 °C for 2 days. All graphite and glassy carbon materials (Carbone–Loraine) were heated to 840 °C for 16 h at 10^{-3} mbar before use.

The Raman system and data treatment

The Raman apparatus used for measuring the spectra consisted of a T-64000 (Jobin Yvon) triple monochromator equipped with a spectraview 2D™ liquid nitrogen-cooled CCD detector. Spectra were excited with the 488 nm line of an Ar^+ laser (Spectra Physics Model 2017) with a constant power of 500 mW in front of the focusing lens. The spectral slit width used was ≈5 cm^{-1} while spectrum integration time was 120 s. Two polarization configurations were employed for recording the spectra of the melt in the 90° scattering geometry: polarized, marked as VV (Vertical polarization of the incident laser line–Vertical analysis of the scattered light) and the depolarized, marked as HV (Horizontal polarization of the incident laser line–Vertical analysis of the scattered light). A complete description of the windowless graphite Raman optical cells[8] and of the optical furnace capable of attaining temperatures up to 1100 °C[9] is given in the references section.

To assess the symmetry of the Raman bands of a fluid, the isotropic $I_{ISO}(\omega)$ and the anisotropic $I_{ANISO}(\omega)$ scattering intensities are given from the relationships

$$I_{ISO}(\omega) = I_{VV}(\omega) - (4/3)\, I_{HV}(\omega) \quad (1)$$

and

$$I_{ANISO}(\omega) = I_{HV}(\omega) \quad (2)$$

 DOI: 10.1039/b111563b

The reduced intensity $R_\sigma(\omega)$ as a function of the measured intensity $I_\sigma(\omega)$ and the Raman shift ω can be calculated from the equation

$$R_\sigma(\omega) = I_\sigma(\omega)\, \omega\, (\omega_0 - \omega)^{-4}\, [n(\omega) + 1]^{-1} \qquad (3)$$

where σ stands for ISO, VV and ANISO, ω_0 is the excitation laser frequency and $[n(\omega) + 1] = [\exp(h\omega c/kT) - 1]^{-1}$ is the Boltzmann thermal population factor. The advantages of using the reduced as well as the ISO and ANISO representation of the spectra have been discussed before.[10]

The optical Raman cell for the NdOF powder investigation consisted of a vitreous silica tube (4 mm o.d., 3 mm i.d.) flame-sealed under vacuum. The micro-Raman facility of the T-64000 Jobin Yvon system was employed to investigate NdOF. Spectra were excited with the 514.5 nm line of a Spectra Physics air-cooled Ar^+ laser (model 163-A42). Laser plasma lines were rejected using a proper interference filter. The excitation beam was directed towards the microscope and focused onto the sample with the use of a beam splitter and a microscope objective of 50×/0.55 (Olympus). Scattered radiation was collected in back-scattering geometry using the same microscope objective and, after passing through the beam splitter and a notch filter, was focused on the slit of the triple monochromator. The standard VV configuration was used for all solid-state samples studied.

Procedure for solubility measurements

The equilibrium studies at different melt compositions and temperatures were carried out in a furnace mounted vertically under an argon filled glove box, making it possible to access the experimental cell from inside without introducing moisture to the cell. The water and oxygen content in the box were < 1 and < 3 ppm, respectively. All handling of purified salts and samples were performed in the box. The cell and furnace assembly is shown in Fig. 1. A graphite lid was placed on top of

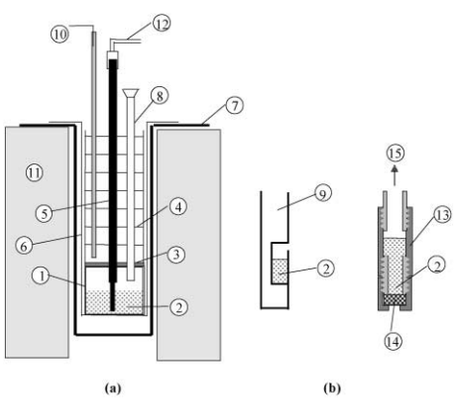

Fig. 1 The experimental set-up. The furnace was mounted under a glove box. (1) glassy carbon crucible; (2) melt; (3) graphite lid; (4) graphite radiation shields; (5) stirring rod; (6) quartz tube; (7) furnace tube; (8) quartz tube for salt and/or oxide additions or steel tube for sampling; (9) graphite ladle for sampling attached to (8); (10) thermocouple; (11) furnace; (12) to motor; (13) graphite sampling device attached to (8); (14) graphite filter; (15) to vacuum pump.

a glassy carbon crucible, graphite radiation shields were mounted on the top of the lid at a regular distance to decrease the vertical temperature gradient in the cell. A glassy carbon tube surrounded the radiation shields to reduce the corrosive actions of fluorides on the quartz cell. The lid and the shields had holes for sample extraction and feeding of salts, stirring unit and thermocouple. Melt samples for chemical analysis were extracted from the melt using graphite ladles or by extracting the melt through a graphite filter with a porosity of 15–40 μm to avoid particles of solid Nd_2O_3, while stirring was performed with a graphite blade connected to an electrical motor *via* a steel rod. The experimental cell was mounted inside a quartz tube, immersed in a Kanthal tube mounted inside the furnace to separate it from the glove box. A brass lid, with holes similar to those in the graphite lid, was positioned on top of the quartz tube to prevent impurities from falling into the cell. The cell was kept in the glove box furnace at 500 °C for several hours in order to remove adsorbed water, before measured quantities of the salts were added to the glassy carbon crucible. The total amount of fluorides used was about 100 g.

In the first experiment pellets of Nd_2O_3 were added to obtain a concentration below the solubility limit. A sample was then extracted for analysis. Then more Nd_2O_3 was added and the procedure repeated until the Nd_2O_3 concentration in the melt was constant. In this way a one-to-one correspondence between added and analysed Nd_2O_3 could be observed until excess Nd_2O_3 had been added. In the next experiment, the equilibration time was recorded by adding Nd_2O_3 in excess and through regular sampling and analysis the change of the dissolved neodymium oxide concentration was observed. Then the equilibrium $Nd_2O_3(s) = Nd_2O_3(dissolved)$ was studied as a function of temperature and melt composition. The oxide content of the extracted samples was determined by a carbothermal method using LECO TC-436 or the newer instrument LECO TC-436DR, as described by Mediaas *et al.*[11,12] Five to seven samples were analysed for each composition, and results are given as a mean value using a standard deviation based on a normal distribution. The samples were chosen from different parts of the solidified samples to avoid any systematic error due to inhomogeneity in the quenched melts.

Results and discussion

Raman data

The binary NdF_3–LiF phase diagram is characterised by a simple eutectic at $x_{NdF_3} = 0.23$ and $T = 738$ °C.[13] Fig. 2 presents

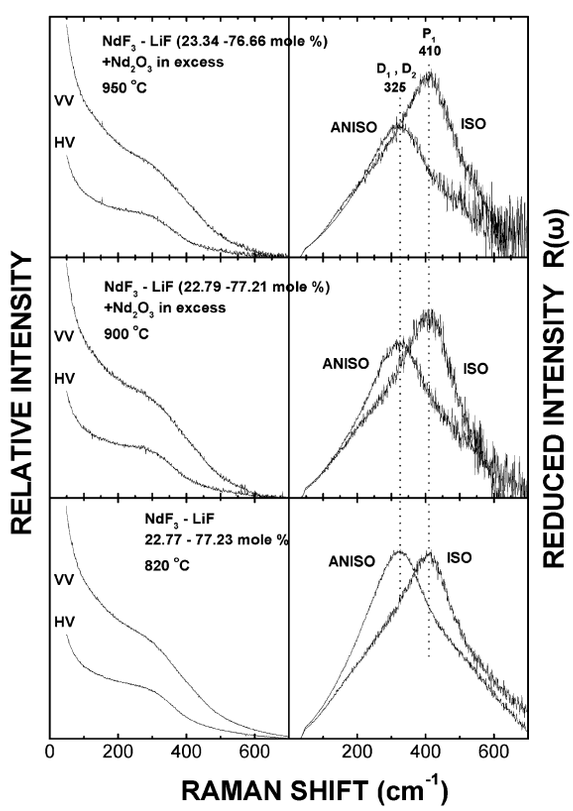

Fig. 2 Raman spectra of molten NdF_3–LiF and NdF_3–LiF–Nd_2O_3 mixtures (Nd_2O_3 in excess). The reduced representation of the isotropic and anisotropic spectra is depicted on the right side of the figure. Spectra conditions: laser wavelength $\lambda_0 = 488$ nm, power 500 mW, slits 5 cm^{-1}, integration time 120 s.

Table 1 Estimated Raman frequencies (cm^{-1}) of the Nd–F and Nd–O bonds for a number of hexafluorides and oxyfluorides [18]

NdF_6^{3-}	$NdOF_5^{4-}$			$NdOF_4^{3-}$		$NdOF_3^{2-}$	
$\nu_1(A_{1g})$	$\nu_1(A_1)$	$\nu_2(A_1)$	$\nu_3(A_1)$	$\nu_1(A_1)$	$\nu_2(A_1)$	$\nu_1(A_1)$	$\nu_2(A_1)$
$\nu_s(NdF_6)$	ν(Nd=O)	ν(Nd–F)[b]	$\nu(NdF_4)$	ν(Nd=O)	$\nu_s(NdF_4)$	$\nu(NdF_3)$	ν(Nd=O)
412	≈560	≈340	≈340	≈670	≈390	≈470	≈740

[b] Fluorine in *trans* position with respect to oxygen.

the Raman spectra of the molten binary NdF_3–LiF eutectic as well as those of the same liquid mixture after the dissolution of small amounts of Nd_2O_3. Polarised (VV) and depolarised (HV) spectra of the liquid eutectic are characterised by an up to ≈400 cm^{-1} extended "liquid wing" without exhibiting any significant structural features. Much more revealing are the spectra in the reduced isotropic and anisotropic form. Taking into account previous Raman studies in the similar YF_3–KF [14] and LnF_3–KF (Ln = La, Ce, Nd, Sm, Dy, Yb) [15] systems, the structure of liquid NdF_3–LiF is dominated by the presence of the poorly defined octahedral NdF_6^{3-} complex anion. This species is identified by the main polarised band P_1 = 412 cm^{-1} and the broad depolarised contour centred at ≈325 cm^{-1} covering D_1 and D_2 bands. The strong polarised band P_1 arises mainly from the $\nu_1(A_{1g})$ "breathing mode" of the NdF_6^{3-} octahedra, while D_1 is close to the bending mode $\nu_5(T_{2g})$. The $\nu_2(E_g)$ asymmetric mode cannot be observed since it is generally weaker than both the symmetric and the bending modes of the octahedral metal halide complexes $[MX_6]^{n-}$. In fact the intensity of the asymmetric mode becomes even weaker at higher temperature.[10,16] The NdF_6^{3-} octahedra are rather distorted, resulting in broad Raman band shapes, due to the strong attraction of the fluorine atoms by the Li^+ cation. The gross spectral features are analogous to those observed for the molten $NdCl_3$–LiCl mixtures.[16]

A very interesting feature of the reduced isotropic and anisotropic spectra is that their intensity is comparable. This strong anisotropic scattering can be interpreted by enhanced Dipole–Induced-Dipole (DID) interactions between neighbouring Nd^{3+} cations, resulting from the polarisability of the neodymium cations, which are not well shielded in fluoride melts in the presence of Li^+. In fact, a similar explanation was proposed to account for the intensity of the anisotropic light scattering, increasing in the sequence Y–La for the LnF_3–KF liquid mixtures having $x(LnF_3) > 0.25$.[15] It was suggested that the higher polarisability of La^{3+} compared to Y^{3+} allows stronger DID interactions between neighbouring La^{3+} cations. Thus, the strong depolarised scattering in the liquid NdF_3–LiF eutectic arises from a combined effect of the small Li^+ cations as well as the first neighbour Nd^{3+} cations of the nearest NdF_6^{3-} octahedra, both acting on the Nd^{3+} cation located at the centre of the NdF_6^{3-} octahedron. Addition of small amounts of Nd_2O_3 to the molten NdF_3–LiF eutectic results in the reduced isotropic and anisotropic spectra also shown in Fig. 2. The energies of the main polarised band P_1 and of the depolarised band contour of D_1 and D_2 remain practically unchanged. More prominent are the changes in the relative intensities of the reduced isotropic and anisotropic scattering, the former clearly dominating the latter. The presence of the oxyfluoride complex ions decreases the already mentioned DID interactions observed in the liquid NdF_3–LiF eutectic, mainly through the better shielding that the oxygen anions offer for the Nd^{3+} cations. In this way, the relative intensities of isotropic and anisotropic scattering can be accounted for. It should be mentioned that with increasing temperature the reduced intensity of the anisotropic $\nu_5(T_{2g})$ band is expected to decrease relative to that of the isotropic $\nu_1(A_{1g})$ for the liquid NdF_3–LiF eutectic. This decrease is justified in view of the diminishing DID polarisability fluctuations with increasing temperature.[15,17] However, the observed effect of temperature on the relative intensities of reduced isotropic and anisotropic scattering for the liquid NdF_3–LiF eutectic at 900 and 950 °C is small compared with the measured variation due to Nd_2O_3 dissolution (Fig. 2) that increases with increasing temperature (see Solubility data section). Furthermore, if the temperature effect was dominant a dramatic influence on the bandwidth would also be expected.

The structure of the molten NdF_3–LiF eutectic is characterised by the presence of poorly defined short-lived octahedral NdF_6^{3-} complex ions. Bands that could clearly be attributed to entities such as Nd_2O_3 or NdOF could not be located in the spectra of the liquid NdF_3–LiF–Nd_2O_3 mixtures. All the above spectral features are suggestive of minor structural changes on Nd_2O_3 dissolution which indicates that the oxyfluoride complexes should be similar to the octahedral NdF_6^{3-}. Probable oxyfluoride complexes conforming to the spectral data are the mononuclear $NdOF_4^{3-}$, $NdOF_5^{4-}$ and the binuclear $Nd_2OF_{10}^{6-}$, $Nd_2OF_9^{5-}$ and $Nd_2OF_8^{4-}$ ions. Although no data are available for the Nd–F and Nd–O bonds hypothetical calculated Raman frequencies are presented in Table 1. These bands are averages based on the known frequencies [18] of M–F and M–O bonds of the metal oxyfluoride complexes relative to the octahedral MF_6 frequencies [M = Cr(VI), Mo(VI), W(VI), Se(VI), Te(VI), Ti(IV), V(IV), Re(VII), U(VI)].

The most probable mononuclear oxyfluoride complexes are $NdOF_4^{3-}$ with the Nd^{3+} cation five-co-ordinated or the six-co-ordinated $NdOF_5^{4-}$. The presence of the six-fold co-ordinated O^{2-}-containing complex should cause a red shift in the energy of the main polarised band relative to the same band for the pure fluoride containing binary mixture (Fig. 2). The six-fold co-ordination for the Nd^{3+} cation is also realised in the binuclear single oxygen-bridged $Nd_2OF_{10}^{6-}$ (F_5Nd–O–NdF_5) complex. Formation of the oxygen bridging bond results in a strengthening of the Nd–F terminal bonds compared to the respective bonds of the mononuclear $NdOF_5^{4-}$. At the same time, the favoured local structure of neodymium is retained. The spectral features shown in Fig. 2 therefore seem to be more compatible with the binuclear $Nd_2OF_{10}^{6-}$ complex due to the minor changes observed in the energy of the Nd–F bonds when adding the oxide. Such highly charged complex anions as $Nd_2OF_{10}^{6-}$, however, are not encountered in molten salt systems. In conclusion, it may therefore be reasonable to assume that $NdOF_5^{4-}$ is the complex ion present.

The solubility data, presented later in the paper, show solubilities of 0.38, 0.22 and 0.15 mol% Nd_2O_3 at 900 °C for the melt compositions 30, 23 and 15 mol% NdF_3, respectively. It is well known from similar systems that it is the MF_x salt that promotes the solubility of its corresponding M_2O_x oxide. The solubility of Nd_2O_3 in pure molten LiF will therefore be very low. Thus the dissolution mechanism of Nd_2O_3 in the molten NdF_3–LiF eutectic can be described by a reaction of the type

$$Nd_2O_3 + NdF_3 + 3(x-1)LiF = 3NdOF_x^{(x-1)-} + 3(x-1)Li^+ \quad (4)$$

This reaction shows that LiF acts as a F^- ion donor only, and that Nd^{3+} ion in solution is needed to support the dissolution process. The number of F^- ions in the Nd–O–F complex must most probably be < 5 due to limitations imposed by the maximum co-ordination number of six for the Nd^{3+} cation.

Subsequent reaction of these $NdOF_x^{(x-1)-}$ oxyfluoride complexes with the NdF_6^{3-} octahedra, for the low oxide containing mixtures, can lead to the formation of single-oxygen bridged binuclear complexes $Nd_2OF_{10}^{6-}$ as discussed above. The absence of bands that could be attributed to NdOF, as an entity in the melt, and the stoichiometry and structural considerations discussed above, suggest that small quantities of Nd_2O_3 when dissolved in the liquid NdF_3–LiF eutectic, result in oxyfluoride complexes such as those indicated.

It is well known that in the gaseous phase anions are polarisable while cations are polarising. However, calculations and experiments show that anions in crystals are different from their free atomic counterparts: they are smaller, less polarisable and more strongly bound. The number and distribution of neighbours also influence the properties of negative ions.[19] In crystals therefore, anionic polarisabilities are not constant but are functions of their environment. The polarisability value for the O^{2-} anion is about twice of that of the F^- anion in MgO and LiF crystals, respectively.[19,20] A similar scaling of the polarisability values for the O^{2-} and F^- anions is anticipated in the liquid state. The binding of oxygen to a trivalent metal cation like Nd^{3+} in $NdOF_x^{(x-1)-}$ or $Nd_2OF_{x+3}^{(x-1)-}$ complex anions is expected to lead to somewhat lower polarisability values ratio, *i.e.* $[a(O^{2-})/a(F^-)] < 2$, compared to those in the MgO and LiF crystals. Based on the above argument, the isoelectronic O^{2-} and F^- anions bound to the trivalent Nd^{3+} cation are expected not to have dramatically different polarisability values.

The identical picture of the spectra of Fig. 2 in the frequency domain and their difference with respect to relative intensities of the reduced isotropic and anisotropic form, give a further indication of the dominant role of the polarisability of the Nd^{3+} cations. Thus the formation of an Nd–O bond which is stronger than the Nd–F bond seems to make the Nd^{3+} cation less prone to DID interactions. This seems to explain the decrease in the intensity of anisotropic scattering.

A calorimetric investigation of the liquid binary NdF_3–KF system showed that a broad minimum is present in the enthalpy interaction parameter λ ($= \Delta H_{mix}/x_{NdF_3} X_{KF}$) at $x_{NdF_3} = 0.2$–0.3. This was explained by the formation of the NdF_6^{3-} complex anion.[21] The phase diagram of the system NdF_3–KF–Nd_2O_3 has also been reported,[22] but structural information related to the addition of the oxide to the binary fluoride melt cannot be obtained. Fig. 3 presents the Raman spectra of the NdF_3–KF liquid eutectic (19 mol% NdF_3, mp 625 °C) as well as the spectra of this liquid mixture after the addition of a small amount of Nd_2O_3. An apparent feature is that the structure of the molten NdF_3–KF eutectic is characterised by the existence of discrete NdF_6^{3-} octahedra.[15] This is identified by the well defined $\nu_1(A_{1g}) \approx 416$ cm^{-1} symmetric stretch and the superimposed, on the "Rayleigh wing", $\nu_5(T_{2g}) \approx 190$ cm^{-1} bond. A reduced representation of the isotropic and anisotropic spectra permits a direct comparison with the respective NdF_3–LiF eutectic spectra of Fig. 2. The main polarized band $P_1 = 423$ cm^{-1} of the KF eutectic exhibits a Full Width at Half Maximum (FWHM) of ≈80 cm^{-1} being much narrower than the $P_1 = 412$ cm^{-1} of the LiF eutectic having a FWHM of ≈290 cm^{-1}. Thus the NdF_6^{3-} octahedra are longer-lived with stronger Nd–F bonds in the KF relative to the LiF system. The observed decrease in the reduced intensity of the anisotropic scattering relative to the isotropic, from the LiF (Fig. 2) to the KF eutectic (Fig. 3), supports the proposed scheme of the less polarizable Nd^{3+} cations in melts with the larger K^+ cations. In this respect, the operation of the DID mechanism in the NdF_3–LiF system seems valid.

Dissolution of a small amount of Nd_2O_3 (1 mol% added) in the NdF_3–KF liquid eutectic, leads to a very similar Raman spectrum. The reduced isotropic and anisotropic form of the spectra depicted in Fig. 3 permits a better discrimination of the influence that the dissolved Nd_2O_3 can have on the structure of the molten NdF_3–KF eutectic. A small decrease is observed in

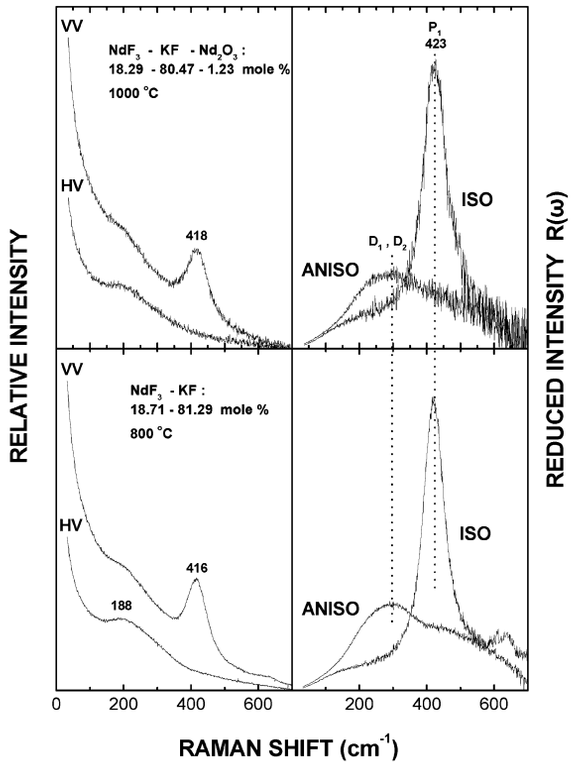

Fig. 3 Raman spectra of molten NdF_3–KF and NdF_3–KF–Nd_2O_3 mixtures. The Nd_2O_3 concentration given is the added amount. The reduced representation of the isotropic and anisotropic spectra is depicted on the right side of the figure. Spectra conditions: laser wavelength $\lambda_0 = 488$ nm, power 500 mW, slits 5 cm^{-1}, integration time 120 s.

Table 2 Assignment of the Raman active modes for rare earth oxyfluorides (REOF)

	Raman shift/cm^{-1}					
REOF	A_{1g}	E_g	A_{1g}	E_g	A_{1g}	E_g
LaOF[a]	103	189	260	353	389	406
NdOF[b]	103	189	272		412	424
GdOF[a]	103	187	295	361	448	452
YOF[a]	140	243	311	378	468	482

[a] Raman data, ref. 23. [b] This work.

the anisotropic scattering intensity relative to the isotropic, accompanied by a small blue shift of the frequency for the main polarized band P_1. The former characteristic could be attributed to diminishing DID interactions while the latter to a strengthening of the Nd–F bonds of the NdF_6^{3-} octahedra. However, both spectral features are also consistent with the existence of oxyfluoride complex anions. According to the arguments presented in the previous section, formation of a Nd–O bond is anticipated to further decrease the already very weak DID interactions between the neighbouring Nd^{3+} cations of the octahedral NdF_6^{3-} in the NdF_3–KF liquid eutectic. This results in a decrease of the anisotropic scattering relative to the isotropic. The shift of the main polarized band to slightly higher frequencies can be thought to arise from the totally symmetric vibration of Nd–F bonds in a species like $Nd_2OF_{10}^{6-}$, stronger than the respective bonds of the NdF_6^{3-} octahedra. This conforms to the presence of the neodymium oxyfluoride complexes, discussed in the previous section.

Raman spectra of some solids were recorded in order to obtain reference data for the interpretation of the liquid melt spectra. NdOF(s) shows the bands given in Table 2. In this table the Raman bands for the similar La, Gd and Y compounds are also given. The assignment of the Raman active modes for

NdOF is based on the structure of the isomorphous rhombohedral REOF (RE = La, Gd, Y).[23] There is little resemblance between the liquid NdF_3–LiF(KF)–Nd_2O_3 spectra and the NdOF data, and a better interpretation of the data in Figs. 2–3 than already presented cannot be given. Raman spectra of the polycrystalline solids of the NdF_3–LiF eutectic and of the NdF_3–LiF–Nd_2O_3 mixture saturated in Nd_2O_3 did not reveal any additional information that could be used to understand the spectra of the liquids. This is most obviously due to the very low solubility of Nd_2O_3 in the solid phases.

Nd_2O_3 solubilities in NdF_3–LiF–MgF_2 melts

The equilibration time for Nd_2O_3 dissolution was measured first and data are presented in Fig. 4. It can be clearly seen that

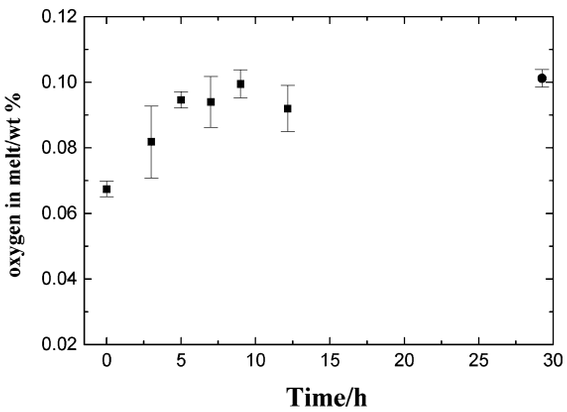

Fig. 4 Oxygen content in the NdF_3–LiF eutectic melt, analysed using a LECO TC-436 instrument, *versus* time (■ = 800, ● = 850 °C). Standard deviations are given as error bars.

saturation is reached after 6–10 h at about 800 °C and an equilibration time of ≈10 h was therefore used in subsequent experiments. The quartz tube had to be renewed after each experiment as the fluoride vapours were found to have attacked the quartz tube. In some experiments, however, an additional vitreous carbon cylinder was mounted on top of the vitreous carbon crucible. This cylinder reduced the corrosion on the silica tube significantly. The wetting of the graphite ladle by the melt was low and it was therefore necessary to have a melt level about 1 cm above the inlet of the ladle to allow samples to be withdrawn easily. The samples withdrawn from the melt were light violet in colour.

In Fig. 5 data for added *versus* analysed Nd_2O_3 are given. The

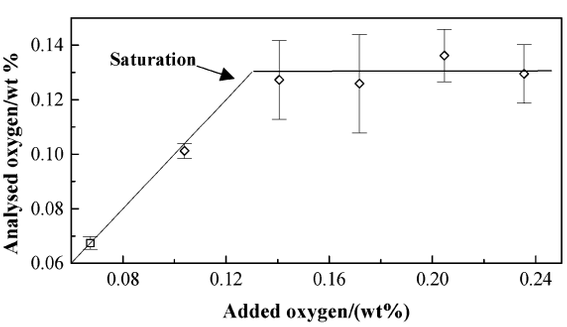

Fig. 5 Oxygen added (theoretical value), as analysed using a LECO TC-436 instrument, (□ = 800, ◇ = 850 °C) when Nd_2O_3 is added to the NdF_3–LiF eutectic. The line with a slope of 1 shows that all the added Nd_2O_3 dissolves before saturation is reached. Standard deviations are given as error bars.

added amount of Nd_2O_3 is equal to the analysed as long as the concentration is below the saturation limit. According to Fig. 6, where the natural logarithm of the oxide concentration in the melt is plotted *versus* $1/T$, straight lines are obtained within the experimental errors for the NdF_3 compositions 15 and

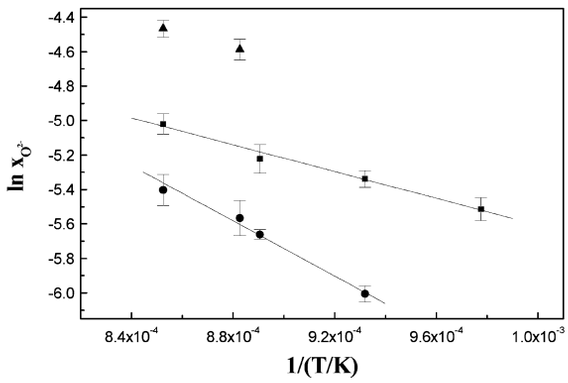

Fig. 6 Oxygen content, $\ln(x_o)$ *versus* $1/T$. The LiF–NdF_3 melts investigated initially contained ●: 15, ■: 23.1, ▲: 30 mol% NdF_3, respectively. The lines were determined by linear regression.

23.1 mol%. The solubility data can be described by the equations:

$$\ln x_{O^{2-}} = -\frac{8006}{T(/\mathrm{K})} + 1.436$$

with correlation coefficient 0.997, standard deviation for the slope 471 and 0.42 for the intercept at 800 < T < 900 °C for the 15 mol% NdF_3 melt and

$$\ln x_{O^{2-}} = -\frac{3879}{T(/\mathrm{K})} - 1.726$$

with correlation coefficient 0.996, standard deviation for the slope 260 and 0.24 for the intercept 0.24 at 750 < T < 900 °C for the 23.1 mol% NdF_3 melt.

The temperature dependence of the solubility can be obtained from the Nd_2O_3 dissolution reaction (4) or simply written as

$$Nd_2O_3(s) = Nd_2O_3\ (\text{dissolved}) \qquad (5)$$

Since the equilibrium constant, K, for reaction (5) is given by

$$\Delta G^\circ = \Delta H^\circ - T\Delta S^\circ = -RT\ln K \qquad (6)$$

where ΔG°, ΔH° and ΔS° are the standard Gibbs energy, enthalpy and entropy changes, respectively, for reactions 4 or 5. If Nd_2O_3 dissolves mainly as $NdOF^{(x-1)-}_{x}$ complexes, then the Nd_2O_3 activity is given by:

$$a^{\mathrm{R}}_{\mathrm{ox}} = x^3_{O^{2-}}\gamma^{\mathrm{R}}_{\mathrm{ox}} \qquad (7)$$

where R indicates a Raoultian standard state, subscript ox stands for neodymium oxide and γ is the Nd_2O_3 activity coefficient in the melt. At the liquid $a^{\mathrm{R}}_{\mathrm{ox}} \equiv 1$ if pure solid Nd_2O_3 is used as a standard state for the activity and $\gamma^{\mathrm{R}}_{\mathrm{ox}}$ is therefore equal to $1/x^3_{O^{2-}}$. Since the solution is very dilute in the oxide even at saturation, $\gamma^{\mathrm{R}}_{\mathrm{ox}}$ will not vary with concentration of Nd_2O_3 below the saturation limit. This means that the temperature variation of $\gamma^{\mathrm{R}}_{\mathrm{ox}}$ at a given concentration of Nd_2O_3 below the saturation limit can be described by

$$\ln\gamma^{\mathrm{R}}_{\mathrm{ox}} = \ln\left(\frac{1}{x^3_{O^{2-}}}\right) = \frac{\Delta\bar{H}_{\mathrm{ox}}(\mathrm{s})}{RT} - \frac{\Delta\bar{S}_{\mathrm{ox(s)}}}{R} \qquad (8)$$

Which, in turn, means that the O^{2-} solubility is given by the equation

$$\ln x_{O^{2-}} = -\frac{\Delta\bar{H}_{ox}(\mathrm{s})}{3RT} + \frac{\Delta\bar{S}_{\mathrm{ox(s)}}}{3R} \qquad (9)$$

and $\Delta\bar{H}_{ox}(s) = \Delta_{fus}H^{\circ}_{ox} + \Delta\bar{H}_{ox}(liq) \approx 200$ and 100 kJ for the 15 and 23.1 mol% NdF_3 melts, respectively. This means that the partial enthalpy of mixing liquid Nd_2O_3 into the NdF_3–LiF binaries, $\Delta\bar{H}_{ox}(l)$, must be considerably positive. This is in agreement with the very low solubilities measured. The linear dependence of the natural logarithm of the oxide concentration in the melt *versus* $1/T$ is also in agreement with the interpretation of the Raman spectra where the most probable species was suggested to be the mononuclear $NdOF_5^{4-}$ instead of the binuclear $Nd_2OF_{10}^{6-}$.

Some Nd_2O_3 solubility data were also recorded in NdF_3–LiF–MgF_2 melts at 860 °C. MgF_2 was added stepwise, to a 30 and a 15 mol% NdF_3 containing liquid mixture and the Nd_2O_3 solubility was determined at each step. The results, shown in Fig. 7, indicate that the Nd_2O_3 solubility decreases somewhat

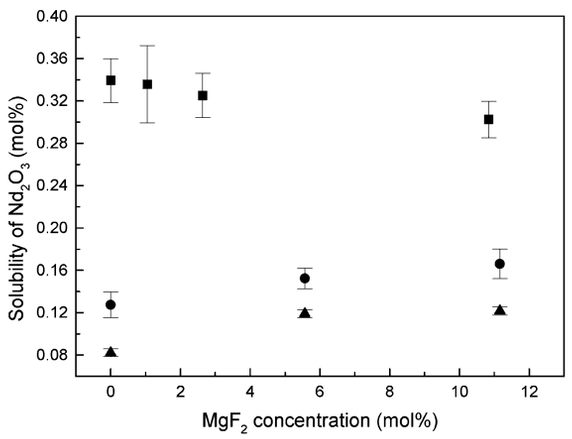

Fig. 7 Nd_2O_3 solubilities in NdF_3–LiF–MgF_2 melts. MgF_2 was added stepwise to binary NdF_3–LiF liquid mixtures saturated with Nd_2O_3. The Nd_2O_3 solubility was determined at each step. ●: 15 mol% NdF_3 at 860 °C, ▲: 15 mol% NdF_3 at 800 °C, ■: 30 mol% NdF_3 at 860 °C.

with increasing MgF_2 concentrations in the 30 and increases in the 15 mol% melt, respectively, but variations are less than expected since liquid MgF_2 shows a considerable (8.5 mol%) MgO solubility.[24] The reaction between MgF_2 and Nd_2O_3 in the mixture indicates that MgO should form if the constituents of the mixture mix ideally. This might be responsible for the low and stable oxide solubility with MgF_2 additions due to MgO precipitation. As can be seen from Fig. 7, this is the case only to a degree. The data make it reasonable to believe that a possible Nd–Mg alloy electrowinning process from an NdF_3–LiF–MgF_2 melt containing Nd_2O_3 dissolved should be possible. The low oxide solubility in the binary fluoride melt is not reduced by MgF_2 additions. The raw material for the process will therefore be Nd_2O_3 and MgF_2. The alloy will form at the cathode and hopefully only $O_2(g)$ at the anode.

Conclusions

The solubility of Nd_2O_3 in NdF_3–LiF–MgF_2 melts is quite low and increases with temperature, as expected from the positive enthalpy of dissolution. When MgF_2 is added to the binary NdF_3–LiF melt only minor changes in the oxide solubility are observed. When dissolving of Nd_2O_3 in the NdF_3–LiF eutectic Raman spectroscopy shows that complexes of the type $NdOF_x^{(x-1)-}$ and $Nd_2OF_{x+3}^{(x-1)-}$ might form in the melt. The most reasonable candidate is $NdOF_5^{4-}$.

Acknowledgements

The authors are indebted to G. Papatheodorou and G. Voyiatzis for providing experimental facilities. G. M. Photiadis thanks K. S. Andrikopoulos for help in various aspects of the Jobin Yvon Raman spectrometer and V. Dracopoulos for help with the Raman measurements of molten fluorides.

References

1 H. Mediaas, G. Photiadis, G. N. Papatheodorou, J. E. Vinstad and T. Ostvold, *Acta Chem. Scand.*, 1997, **51**, 8.
2 A. F. Vik, V. Dracopoulos, G. N. Papatheodorou and T. Østvold, *J. Alloys Compds.*, 2001, **321**, 284.
3 A. F. Vik, V. Dracopoulos, N. Papatheodorou and T. Østvold, *J. Chem. Soc., Dalton Trans.*, 2001, 2164.
4 E. Robert, J. E. Olsen, V. Danek, E. Tixhon, T. Ostvold and B. Gilbert, *J. Phys. Chem. B*, 1997, **101**, 9447.
5 J. E. Murphy, D. K. Dysinger and M. F. Chambers, *Light Metals*, 1995, 1313.
6 E. Morrice and T. A. Henrie, *Bull.-U.S. Bur. Mines*, 1966, 6957.
7 E. Morrice, E. S. Shedd and T. A. Henrie, *Bull.-U.S. Bur. Mines*, 1968, 7146.
8 B. Gilbert and T. Matterne, *Appl. Spectrosc.*, 1990, **44**, 299 and references therein.
9 V. Dracopoulos and G. N. Papatheodorou, *Proc. XI Symp. Molten Salts*, 1998, **98–11**, 544.
10 M. H. Brooker and G. N. Papatheodorou, in *Advances in Molten Salt Chemistry*, eds. G. Mamantov and C. B. Mamantov, 1983, vol. 5, p. 27.
11 H. Mediaas, J. E. Vindstad and T. Østvold, *Light metals*, 1996, 1129.
12 H. Mediaas, J. E. Vindstad and T. Østvold, *Acta Chem. Scand.*, 1997, **51**, 501.
13 R. E. Thoma, G. D. Brunton, R. A. Penneman and T. K. Keenan, *Inorg. Chem.*, 1970, **9**, 1096.
14 V. Dracopoulos, B. Gilbert, B. Borresen, G. M. Photiadis and G. N. Papatheodorou, *J. Chem. Soc., Faraday Trans.*, 1997, **93**, 3081.
15 V. Dracopoulos, B. Gilbert and G. N. Papatheodorou, *J. Chem. Soc., Faraday Trans.*, 1998, **94**, 2601.
16 G. M. Photiadis, B. Borresen and G. N. Papatheodorou, *J. Chem. Soc., Faraday Trans.*, 1998, **94**, 2605.
17 G. N. Papatheodorou, S. G. Kalogrianitis, T. G. Mihopoulos and E. A. Pavlatou, *J. Chem. Phys.*, 1996, **105**, 2660.
18 K. Nakamoto, in *Infrared and Raman Spectra of Inorganic and Coordination Compounds, Part A: Theory and Applications in Inorganic Chemistry*, John Wiley & Sons, Inc., New York, 5th edn., 1997.
19 C. Domene, P. W. Fowler, P. Jemmer and P. A. Madden, *Chem. Phys. Lett.*, 1999, **299**, 51.
20 P. W. Fowler and N. C. Pyper, *Proc. R. Soc.*, 1985, **A398**, 377.
21 G. Hatem and M. Gaune – Escard, *J. Chem. Thermodyn.*, 1993, **25**, 219.
22 A. B. Maimasov, E. I. Ardashnikova and B. A. Popovkin, *Zh. Neorg. Khim.*, 1996; P. W. Fowler and N. C. Pyper, *Proc. R. Soc.*, 1985, **A398**, 377; P. W. Fowler and N. C. Pyper, *Proc. R. Soc.*, 1985, **41**, 1230.
23 J. Holsa, B. Piriou and M. Rasanen, *Spectrochim. Acta*, 1993, **49A**, 465.
24 R. A. Sharma, *J. Am. Ceram. Soc.*, 1988, **71**, 272–276.